Ab Initio Studies of ClO_x Reactions: VI. Theoretical Prediction of Total Rate Constant and Product Branching Probabilities for the $HO_2 + ClO$ Reaction

Z. F. Xu, R. S. Zhu, and M. C. Lin*

Department of Chemistry, Emory University, Atlanta, Georgia 30322

Received: September 24, 2002; In Final Form: December 13, 2002

The reaction of HO_2 with ClO has been investigated by ab initio molecular orbital and variational transition state theory calculations. The geometric parameters of the reaction system $HO_2 + ClO$ were optimized at the B3LYP and BH&HLYP levels of theory with the basis set 6-311+G(3df,2p). Both singlet and triplet potential energy surfaces were predicted by the modified Gaussian 2 (G2M) method. On the singlet surface, the reaction forms two HOOOCl isomers lying below the reactants by 20 kcal/mol. Their stabilization contributes significantly to the observed overall $HO_2 + ClO$ rate constant. The predicted high- and low-pressure association rate constants for the 150−600 K range can be represented by $k^\infty = 9.04 \times 10^{-17}\ T^{1.22} \exp(897/T)$ cm^3 molecule^{-1} s^{-1} and $k^0 = 9.33 \times 10^{-24}\ T^{-3.45} \exp(472/T)$ cm^6 molecule^{-2} s^{-1} for N_2 as the third-body. Dissociation of these excited HOOOCl intermediates produces HO + ClOO, HCl + $^1O_3$, HOCl + $^1O_2$, and HO + OClO as minor products via multistep mechanisms. On the triplet surface, formation of HOCl + $^3O_2$ dominates; it occurs via a long-lived $O_2H\cdots OCl$ complex with 3.3 kcal/mol binding energy. The complex decomposes to give the product pairs with a small (0.1 kcal/mol) barrier. The predicted rate constant can be represented by $k(HOCl + {}^3O_2) = 1.64 \times 10^{-10}\ T^{-0.64} \exp(107/T)$ cm^3 molecule^{-1} s^{-1} in the temperature range 150−1000 K. The total rate constants predicted for 1−760 Torr N_2 pressure exhibit a strong negative temperature dependence below 1000 K. In the 200−400 K range, where most kinetic data have been obtained, the agreement between theory and experiment is excellent. For combustion applications, rate constants for all bimolecular product formation channels have been predicted for the 500−2500 K temperature range.

I. Introduction

Both ClO and HO_2 radicals are present in the Freon-polluted stratosphere.[1] The kinetics and mechanism for their interaction, critical to the prediction of the extent of O_3 destruction, have been investigated by many groups.[2−14] The reaction of $HO_2 +$ ClO may in principle take place by a number of pathways by direct abstraction or by indirect association/decomposition processes involving excited intermediates:

$$HO_2 + ClO \rightarrow HOCl + O_2 \quad (1)$$

$$\rightarrow HOOOCl^* \rightarrow HOCl + O_2 \quad (2)$$

$$\rightarrow HCl + O_3 \quad (3)$$

$$\rightarrow HO + ClOO, \quad (4)$$

$$\rightarrow HOOClO^* \rightarrow HOCl + O_2 \quad (5)$$

$$\rightarrow OH + OClO \quad (6)$$

where $*$ denotes excited intermediates.

The kinetics of the $HO_2 + ClO$ reaction was first investigated by Reimann and Kaufman[2] in 1978 using the discharge-flow method at room temperature, and its rate constant was measured to be $(3.8 \pm 0.1) \times 10^{-12}$ cm^3 molecule^{-1} s^{-1} at 298 K. They monitored HO_2 with OH-LIF (laser induced fluorescence) following the NO titration reaction, $HO_2 + NO \rightarrow OH + NO_2$, in the presence of an excess amount of ClO generated by the $Cl + O_3$ reaction. Howard and co-workers[3] in 1979 employed the LMR (laser magnetic resonance) technique in the temperature range 235−393 K by monitoring both reactants using a discharge flow reactor under low-pressure conditions ($P = 0.8$−3.4 Torr) and obtained the rate constant $3.3 \times 10^{-11} \exp(-850/T) + 4.5 \times 10^{-11}\ (T/300)^{-3.7}$ cm^3 molecule^{-1} s^{-1}. The ClO radical was generated by both $Cl + Cl_2O$ and $Cl + O_3$ reactions. At nearly the same time, Leck et al.[4] reported their room-temperature kinetic data, $(4.5 \pm 0.9) \times 10^{-12}$ cm^3 molecule^{-1} s^{-1}, on HOCl formation by detecting it mass-spectrometrically in a discharge-flow study. The HO_2 radical was produced by both $H + O_2 + M$ and $Cl + H_2O_2$ reactions, whereas the ClO radical was produced by the reaction of Cl atoms with O_3. By using $Cl + Cl_2O$ or OClO to generate ClO, they were able to determine the yield of $HCl + O_3$, formed by reaction 2 above, to be less than 2% of HOCl. Cox and co-workers[5,6] investigated the reaction with other related processes near ambient T and P conditions by modulated-photolysis of mixtures of H_2, O_2, Cl_2 (or Cl_2O), and N_2 aided by kinetic modeling and gave rate constant $(5.4 \pm 4) \times 10^{-12}$ cm^3 molecule^{-1} s^{-1} in 1981[5] and $(6.2 \pm 1.5) \times 10^{-12}$ cm^3 molecule^{-1} s^{-1} in 1986.[6] Their results corroborated the finding of Leck et al. on both HOCl and HCl yields. Finkbeiner et al.[9] measured the products of the reaction by matrix-isolation/FTIR spectroscopy at a total pressure of 700 Torr and at 210, 240, 270, and 300 K. Their result shows that the $HOCl + O_2$ product channel is a major pathway and the branching ratio of $HCl + O_3$ is <5%. Recently, Nickolaisen and co-workers[10] studied the kinetics of the title reaction using the flash photolysis/ultraviolet absorption technique over the temperature range 203−364 K and the pressure range 50−700 Torr of N_2. They described the rate constant by the expression

* To whom correspondence should be addressed. E-mail: chemmcl@emory.edu.

10.1021/jp0221237 CCC: $25.00
Published on Web 04/10/2003

$k(T) = 2.84 \times 10^{-12} \exp[(312 \pm 60)/T]$ cm^3 molecule^{-1} s^{-1}. At almost same time, Knight and co-workers[11] published their experimental result for the reaction using the discharge-flow/mass-spectrometry technique at the total pressure 1.1−1.7 Torr of He in the temperature range 215−298 K. They expressed the rate constant as $k(T) = (7.1 \pm 0.4) \times 10^{-12} \exp[(-16 \pm 17)/T]$ cm^3 molecule^{-1} s^{-1} and indicated HOCl was the only product of the reaction and no evidence for HCl + O_3 formation at any temperature or pressure in their study. These experimental results will be fully cited and compared with our predicted values later.

In addition, there are four theoretical papers on the mechanism and kinetics of the HO_2 + ClO reaction. In 1986, Mozurkewich[12] proposed that the reaction proceeded via a HO_2-ClO intermediate and calculated the rate constants by RRKM theory. Toohey and Anderson[13] reported in 1989 a transition state, connecting the reactants with the HOCl and O_2 products on a triplet surface, at the HF and MP2 levels of theory with the 6-31G(d, p) basis set. They suggested a dual mechanism dominated by direct hydrogen abstraction at high temperatures and by elimination from a stable cyclic OClOOH intermediate at lower temperatures. In 1994, Buttar and Hirst[14] studied the reaction via both the triplet and singlet reaction paths. The geometries were optimized at the MP2/6-31G(d,p) level, and the barriers were determined at the MP4/6-311G(d,p) level. They indicated that the HO_2 + ClO reaction proceeded via a multistep reaction mechanism on the singlet surface and via a direct hydrogen-abstraction mechanism on the triplet surface. In addition to their experimental work, Nickolaisen and co-workers[10] also studied the reaction theoretically; they optimized the minima and saddle points of the reaction on the singlet surface at the B3LYP/6-311++G(3df,3pd) level and on the triplet surface at both MP2/6-31G(d) and CCSD(T)/6-31G(d) levels. They confirmed that the direct hydrogen-abstraction reaction proceeded mainly through a weak hydrogen-bonded intermediate on the triplet surface and that the rather stable HOOOCl intermediate might play an important role in the overall kinetics. To date, no successful attempts have been made to predict the total rate constant and the relative importance of the direct abstraction vs the stabilization of the potentially stable HOOOCl intermediate whose photochemistry may be relevant to the global O_3-destruction process.

In one of our recent papers on ClO_x radical reactions[15−17] with OH, we have reported the results for OH + OClO,[17] which was shown theoretically to produce near unit yield of HOCl + O_2, in full agreement with the experimental result of Poulet et al.[18] The OH + OClO reaction is related to the reverse of reaction 6 shown above; however, it may or may not be directly related to the kinetics reported by various investigators referenced herein. As shown in the above reaction scheme, there are five new reaction paths available to the title reaction system which are not accessible to the OH + OClO reaction. In this study, we examine in full detail the potential contributions from all possible reaction channels by mapping the complete potential energy surface of the system using the G2M method.[19] The rate constants for all major product channels will be calculated with appropriate statistical theories as will be described later.

II. Computational Methods

The geometric parameters of the reactants, products, transition states, and molecular complexes on the singlet and triplet potential energy surfaces (PES) of the HO_2 + ClO system were optimized at the B3LYP/6-311+G(3df, 2p) level of theory.[20,21] Among these species, TS9 and LM3 on the triplet PES were investigated by several other higher level methods because their structures could not be located at the B3LYP level of theory. All of the stationary points have been identified for local minima and transition states by vibrational analysis. Intrinsic reaction coordinate analyses[22] have been performed to confirm the connection between transition states and designated reactants, products or intermediates. Based on the optimized geometries, higher level single-point energy calculations of the stationary points were performed by the G2M(CC2) method,[19] which calculates the base energy at the MP4/6-311G(d, p) level of theory and improves it with the expanded basis set and coupled cluster corrections as well as a "higher level correction (HLC)". All electronic structure calculations were performed with Gaussian 98 program.[23]

TABLE 1: Optimized Geometric Parameters of Reactants and Products (Bond Length in Angstroms and Angles in Degrees)

species		B3LYP/6-311+G(3df,2p)	expt.[27−31]
HOO (^{2}A")	R_{HO}	0.975 (0.960)[a]	0.971
	R_{OO}	1.324 (1.301)	1.331
	θ_{HOO}	105.5 (106.1)	104.3
ClO ($^2\Pi$)	R_{ClO}	1.576 (1.560)	1.570
ClOO(^{2}A")	R_{ClO}	2.250	1.83
	R_{OO}	1.193	1.23
	θ_{ClOO}	116.3	110.0
OClO ($^2B_1$)	R_{OCl}	1.479	1.471
	θ_{OClO}	117.3	117.6
HOCl (^{1}A′)	R_{HO}	0.966	0.964
	R_{OCl}	1.700	1.689
	θ_{HOCl}	103.7	103.0
O_3($^1A_1$)	R_{OO}	1.251	1.278
	θ_{OOO}	118.3	116.8
O_3($^3B_1$)	R_{OO}	1.291	
	θ_{OOO}	129.6	
OH ($^2\Pi$)	R_{OH}	0.974	0.971
HCl	R_{HCl}	1.280	1.275
$^1O_2$	R_{OO}	1.203	
$^3O_2$ ($^3\Sigma^-_g$)	R_{OO}	1.203	1.208

[a] The values in the parenthesis are optimized at the BH&HLYP/6-311+G(3df, 2p) level.

The rate constant for the barrierless abstraction reaction was calculated by the VARIFLEX program[24] based on the microcanonical Rice−Ramsperger−Kassel−Marcus (RRKM) theory.[25] The component rates were evaluated at the E/J-resolved level and the pressure dependence was treated by one-dimensional master equation calculations using the Boltzmann probability of the complex for the J distribution. For the barrierless association/decomposition process, either the individual points or the fitted Morse function, $V(R) = D_e\{1 - \exp[-\beta(R - R_e)]\}^2$, was used to represent the minimum potential energy path (MEP) as will be discussed later. Here, D_e is the bonding energy excluding zero-point vibrational energy for an association reaction, R is the reaction coordinate (i.e., the distance between the two bonding atoms), and R_e is the equilibrium value of R at the stable intermediate structure.

For the coupling of different accessible reaction paths via long-lived intermediates, we have employed the ChemRate program of NIST[26] to calculate the rate constants. Predicted rate constants will be compared with all existing experimental results.

III. Results and Discussion

A. Potential Energy Surfaces and Reaction Mechanism. Tables 1 and 2 list the calculated geometry parameters, moments of inertia, and frequencies of the reactants and products, as well as the available experimental values for them. From Table 1, it can be seen that the bond lengths and bond angles in these

TABLE 2: Moments of Inertia and Vibrational Frequencies of the Reactants and Products Predicted at the B3LYP Level with the 6-311+G(3df,2p) Basis Set

	B3LYP/ 6-311+G(3df,2p)		expt.[28−32]
species	I_a, I_b, I_c (a.u.)	frequencies (cm^{-1})	frequencies (cm^{-1})
HOO (^{2}A")	2.8, 53.2, 56.1 (2.7, 51.4, 54.2)[a]	1171, 1443, 3612 (1263, 1521, 3834)	1098,1392, 3436
ClO ($^2\Pi$)	97.3, 97.3 (95.3, 95.3)	861.5 (880)	853
ClOO(^{2}A")	24.0, 410.7, 434.7	113, 326, 1594	192, 408, 1442
OClO ($^2B_1$)	35.2, 182.4, 217.6	450, 966, 1117	447, 945, 1110
HOCl (^{1}A′)	2.9, 120.2, 123.2	739, 1261, 3786	725,1267, 3794
$O_3(^1A_1)$	15.6, 131.7, 147.4	754, 1214, 1265	705, 1043, 1110
$O_3(^3B_1)$	11.5, 155.8, 167.4	576, 748, 1041	
OH ($^2\Pi$)	3.2, 3.2	3721	3735
HCl	5.7, 5.7	2947	2889
$^1O_2$	41.3, 41.3	1634	
$^3O_2$ ($^3\Sigma_g^-$)	41.3, 41.3	1645	1580

[a] The values in the parenthesis are optimized at the BH&HLYP/6-311+G(3df, 2p) level.

species optimized at the B3LYP/6-311+G(3df,2p) level are close to the experimental values[27−31] except those of ClOO. The differences in the bond length and bond angle of ClOO between the predicted and the experimental values reach 0.420 Å and 6.3°, respectively. These deviations could be attributed to the large electron correlation effect in the ClOO radical. When QCISD/6-311G(d, p) was used to optimize the geometry of ClOO, the above differences were reduced to 0.15 Å and 5.2° with the Cl−O bond length closer to the experimental one. From the frequencies of these species in Table 2, one sees that most of the calculated values at the B3LYP/6-311+G(3df,2p) level are in good agreement with the experimental data, but for O_3, the predicted values are overestimated by 6% to 16% compared with the experimental ones, the differences may be ascribed to its diradical and multireference character which may not be well described by the B3LYP/6-311+G(3df,2p) method. The geometries of these intermediates optimized at the B3LYP/6-311+G(3df,2p) level of theory are shown in Figure 1, whereas those of the transition states optimized at the same level are displayed in Figure 2. The structures of TS9 and LM3 optimized at the BH&HLYP, MP2, QCISD, and CCD levels of theory are drawn in Figure 3. The vibrational frequencies and moments of inertia are summarized in Table 3 for these intermediate complexes and transition states. The energy diagrams obtained at the G2M//B3LYP/6-311+G(3df,2p) level are presented in Figure 4, parts a−c. In Figure 4c, the values of the HOCl + $^3O_2$ products channel were obtained at the G2M//BH&HLYP/6-311+G(3df,-2p) level which will be discussed in the following section. Table 4 compares the experimental and calculated heats of formation for key species including HOOOCl.

1. Singlet Reaction Channels. (a) HOOOCl-1, HOOOCl-2, and Their Isomerization. HOOOCl-1 and HOOOCl-2 can be barrierlessly formed by the association of HO_2 with ClO as shown in Figure 1. Examining the structures of HOOOCl-1 and HOOOCl-2, one sees that both isomers are very similar except the position of the H atom as revealed by the difference in the dihedral angle ∠HOOO, −97.1 and 78.0°, respectively, in HOOOCl-1 and HOOOCl-2. These two isomers were calculated by Peterson and Francisco,[35] by Phillips and Quelch,[36] by Rohlfing,[37] and recently by Nickolaisen et al.[10] at the CCSD-(T)/cc-pVTZ+d, MCSCF (using the McLean−Chandler atomic basis for chlorine with the addition of two sets of d polarization functions, Dunning−Hay atomic basis with a single set of d polarization functions for oxygen and with a single set of p

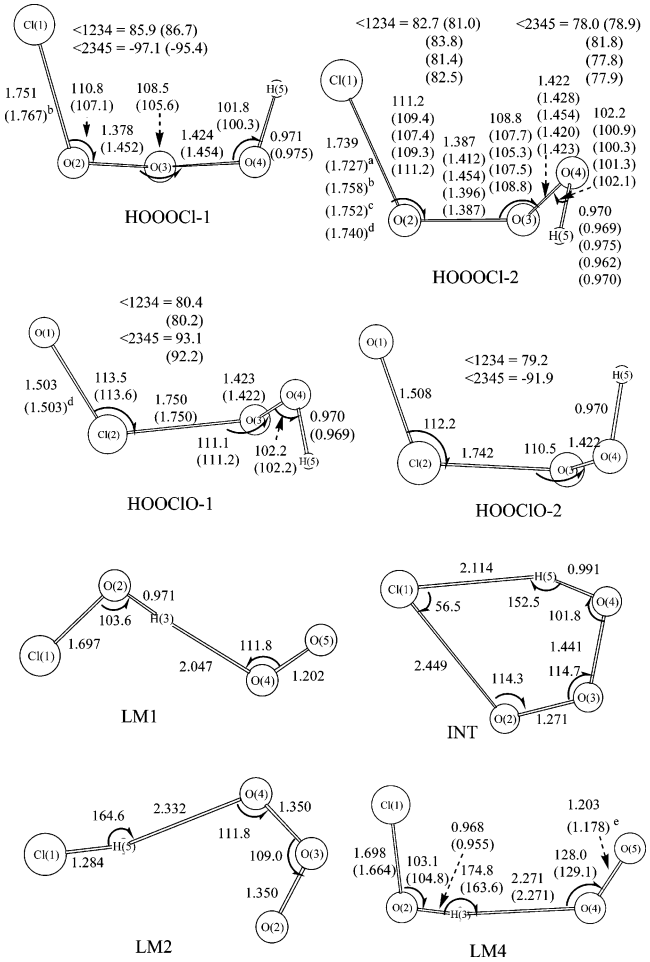

Figure 1. Geometries of complexes and intermediate (Å and degree) optimized at the B3LYP/6-311+G(3df,2p) level. The values in the parenthesis from top to bottom were calculated at the (a) CCSD(T)/cc-pVTZ+d calculation by Peterson and Francisco,[35] (b) MCSCF(CAS) calculation by Phillips and Quelch,[36] (c) QCISD(FU)/6-311G(2d,2p) calculation by Rohlfing,[37] (d) B3LYP/6-311++G(3df,3pd) calculation by Nickolaisen et al.,[10] and (e) BH&HLYP/6-311+G(3df,2p) calculation in this paper.

polarization functions for hydrogen), QCISD(FU)/6−311G(2d,-2p), and B3LYP/6-311++G(3df,2pd) levels, respectively. For the isomer HOOOCl-1, our predicted geometry is close to that obtained by Phillips and Quelch[36] at the MCSCF level; the deviation in the bond lengths and bond angles between ours and Phillips and Quelch's are less than 0.075 Å and 3°, respectively. For HOOOCl-2, the bond lengths calculated in this work are within the corresponding values given by the above authors,[10,35−37] which are close to the values obtained at the CCSD(T)/cc-pVTZ+d and QCISD(FU)/6−311G(2d,2p) levels; they are, however, slightly shorter than those obtained at the MCSCF level. The bond angles calculated in this work are also in good agreement with those obtained at the CCSD(T)/cc-pVTZ+d and QCISD(FU)/6-311G(2d, 2p) levels, but they are larger than those data obtained by MCSCF by 2−4°.

The isomerization between HOOOCl-1 and HOOOCl-2 occurs mainly through the rotation of the OH group around the O(3)−O(4) bond, with a barrier of 5.2 kcal/mol. The corresponding transition state TS3 is presented in Figure 2. Comparing with the geometric parameters of both isomers, the dihedral angle ∠2345 of TS3 becomes −22.1° and there are also a slight decrease in the O(2)−O(3) bond and some increases in the Cl−O and O(3)−O(4) bonds as well as all of the bond angles.

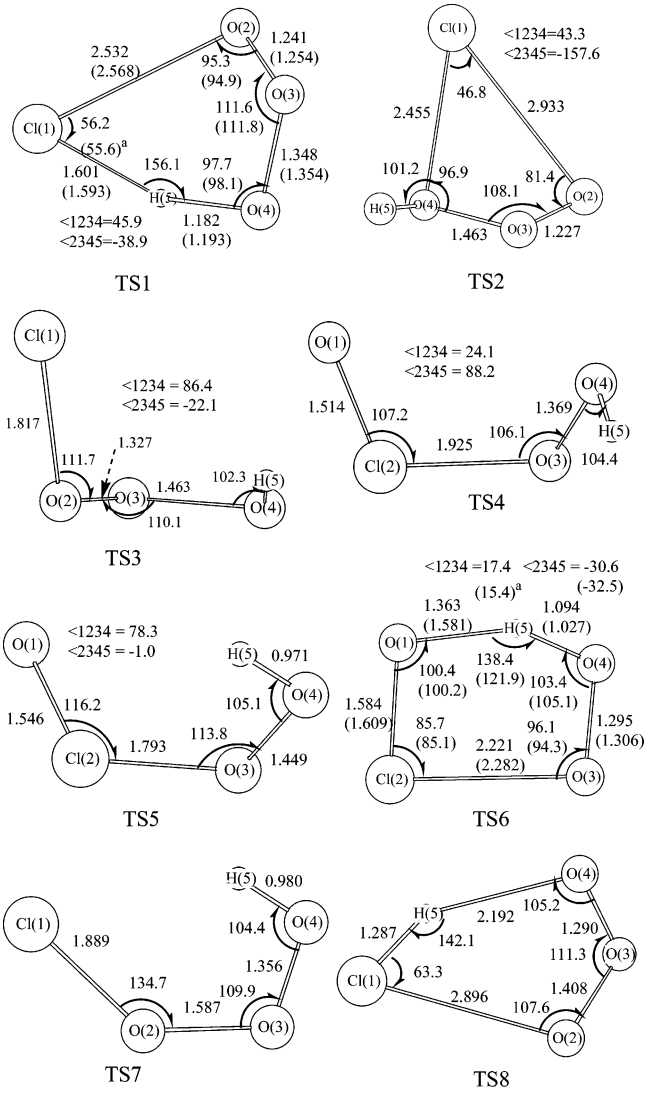

Figure 2. Geometries of transition states (angstroms and degree) optimized at the B3LYP level with 6-311+G(3df,2p) basis set. (a) B3LYP/6-311+G(3df,3pd) calculation by Nickolaisen et al.[10]

The heats of formation of HOOOCl-1 and HOOOCl-2 at 0 K have been calculated to be 7.9 ± 0.8 kcal/mol at the G2M level on the basis of the enthalpy change from the reactants, as shown in Table 4. The error given reflects only those of the reactants. This value is 1.2 and 4.6 kcal/mol lower than those predicted by Francisco and Sander[40] and Nickolaisen and co-workers,[10] respectively. Similar calculations using the enthalpy changes from HOOOCl to HO + ClOO and HO + OClO gave rise to 8.4 ± 0.7 and 6.1 ± 1.9 kcal/mol, respectively. From Figure 4, one can see that HOOOCl is at least about 20 kcal/mol lower than reactants, TS1, TS2, and HO + ClOO. Accordingly, HOOOCl might be quite stable under the stratosphere condition as was suggested by Nickolaisen et al.[10] also.

(b) HCl + $^1O_3$ Formation. The formation of HCl + $^1O_3$ from HOOOCl-1 occurs via TS1, in which the H atom migrates to the Cl atom, followed by the Cl(1)−O(2) bond breaking. The structure of TS1 is displayed in Figure 2. Apparently, in the twisted five-membered ring transition state, the forming Cl−H bond length shortens to 1.601 Å, which is 0.321 Å longer than the bond length of the HCl molecule predicted at the same level; the Cl(1)−O(2) and H−O bonds stretch by 0.781 and 0.211 Å, respectively, compared to those of HOOOCl-1; meanwhile, both the O(2)−O(3) and O(3)−O(4) bonds decrease by 0.136 and 0.076 Å, respectively, and the bond angle ∠OOO increases

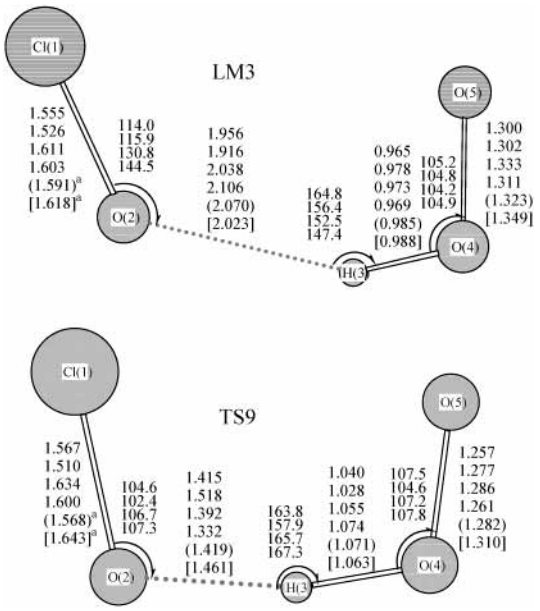

Figure 3. Geometries of TS9 and LM3 (angstroms and degree) optimized at several levels of theory. The numbers are in the order from top to bottom: BH&HLYP/6-311+G(3df,2p), MP2/6-311+G(3df,2p), QCISD/6-311++G(d,p), CCD/6-311++G(d,p), (a) Calculated values by Nickolaisen et al.,[10] MP2/6-31G(d) in parentheses and CCSD(T)/6-31G(d) in brackets.

by about 3°, and the structure of the OOO moiety in TS1 is close to that of $^1O_3$. From Figure 4a, one can see that the forward and reverse barriers of this reaction channel are 23.8 and 22.5 kcal/mol, respectively. The vibrational analysis result shows the imaginary frequency of TS1 to be 1098 cm^{-1}, and its vector points to HOOOCl-1 positively and to HCl + $^1O_3$ negatively.

(c) HOCl + $^1O_2$ Formation. There are two reaction channels producing HOCl and $^1O_2$ as shown in Figure 4, parts a and b. In the first channel, the reaction proceeds via the transition state TS2 from HOOOCl-2 to the products HOCl + $^1O_2$. The transition state is approximately a twisted four-membered ring structure with an imaginary frequency of 167 cm^{-1}, as displayed in Figure 2. The breaking bonds Cl−O(2) and O(3)−O(4) are elongated to 2.933 and 1.463 Å, respectively, at the transition state. Meanwhile, the forming bond Cl−O(4) is shortened to 2.455 Å, which is 0.755 Å longer than that of HOCl predicted at the same level. Because this transition state corresponds to the heavy atom (Cl) migrating from one oxygen atom to another one, it is located on a flatter potential energy surface and has a lower imaginary frequency, which is confirmed by IRC. At the G2M level, TS2 lies above the reactants by 1.3 kcal/mol, the forward and reverse potential barriers of this reaction channel are 21.6 and 22.0 kcal/mol, respectively.

The second reaction channel, a multiple-step process via three transition states, is the reverse of the OH + OClO reaction.[17] To produce HOCl + $^1O_2$ from HOO + ClO, the reaction proceeds by the following sequence: HOO + ClO → TS4 → HOOClO-1 → TS5 → HOOClO-2 → TS6 → LM1 → HOCl + $^1O_2$, as shown in Figure 4b. In the first step, the Cl atom of ClO approaches the terminal oxygen atom of HOO to form HOOClO-1 via TS4. The distance of Cl(2)−O(3) is 1.925 Å at the first transition state and 1.750 Å at the first intermediate, as shown in Figures 1 and 2. In the second step, the O−H bond rotates around the O(3)−O(4) bond inward via TS5 to form HOOClO-2. The two isomers and TS5 have similar geometric parameters except the dihedral angle ∠2345 which is 93.1°, −1.0°, and −91.9° for HOOClO-1, TS5, and HOOClO-2, respectively. In the third step, with the O(1) and H(5) atoms

TABLE 3: Moments of Inertia and Vibrational Frequencies of the Intermediate Complexes and Transition States Predicted at the B3LYP6-311+G(3df,2p) Level

	B3LYP/6-311+G(3df,2p)	
species	I_a, I_b, I_c (a.u.)	frequencies (cm^{-1})
^{1}HOOOCl-1	102.2, 513.1, 574.9	155, 319, 422, 525, 595, 764, 924, 1406, 3719
^{1}HOOOCl-2	99.8, 519.2, 575.3	148, 324, 427, 537, 606, 752, 916, 1410, 3723
^{1}HOOClO-1	103.2, 466.4, 515.6	137, 255, 356, 432, 489, 871, 1007, 1401, 3735
^{1}HOOClO-2	109.8, 446.0, 506.6	125, 271, 356, 452, 503, 874, 995, 1411, 3732
^{3}INT	145.8, 567.2, 713.0	166, 179, 225, 473, 555, 789, 1190, 1497, 3318
LM1	78.5, 1160.3, 1238.8	22, 40, 75, 168, 294, 743, 1327, 1631, 3690
LM2	135.0, 1103.6, 1238.6	40, 43, 69, 222, 279, 574, 613, 1102, 2898
LM3[a]	123.2, 816.8, 918.7	31, 49, 112, 186, 445, 904, 1279, 1573, 3752
LM4	136.0, 1063.9, 1199.9	4, 18, 64, 87, 177, 743, 1281, 1647, 3763
TS1	143.0, 495.8, 618.8	i1098, 202, 379, 464, 748, 902, 1042, 1245, 1570
TS2	151.2, 538.6, 660.6	i167, 189, 289, 500, 533, 702, 1240, 1375, 3657
TS3	102.6, 532.4, 592.9	i400, 167, 316, 514, 560, 818, 929, 1414, 3723
TS4	136.0, 395.6, 516.4	i134, 198, 348, 468, 542, 964, 1021, 1432, 3676
TS5	103.2, 456.7, 507.2	i441, 154, 311, 395, 563, 818, 1003, 1391, 3724
TS6	145.4, 369.5, 508.9	i789, 230, 250, 505, 526, 854, 1205, 1465, 2023
TS7	104.8, 624.2, 729.0	i960, 108, 230, 346, 449, 509, 983, 1445, 3556
TS8	143.3, 734.9, 868.8	i116, 46, 115, 249, 328, 407, 578, 1096, 2853
TS9[a]	133.8, 525.3, 659.1	i1086, 125, 139, 342, 771, 849, 1128, 1588, 1837

[a] Those structures are optimized at the BH&HLYP/6-311+G(3df, 2p) level.

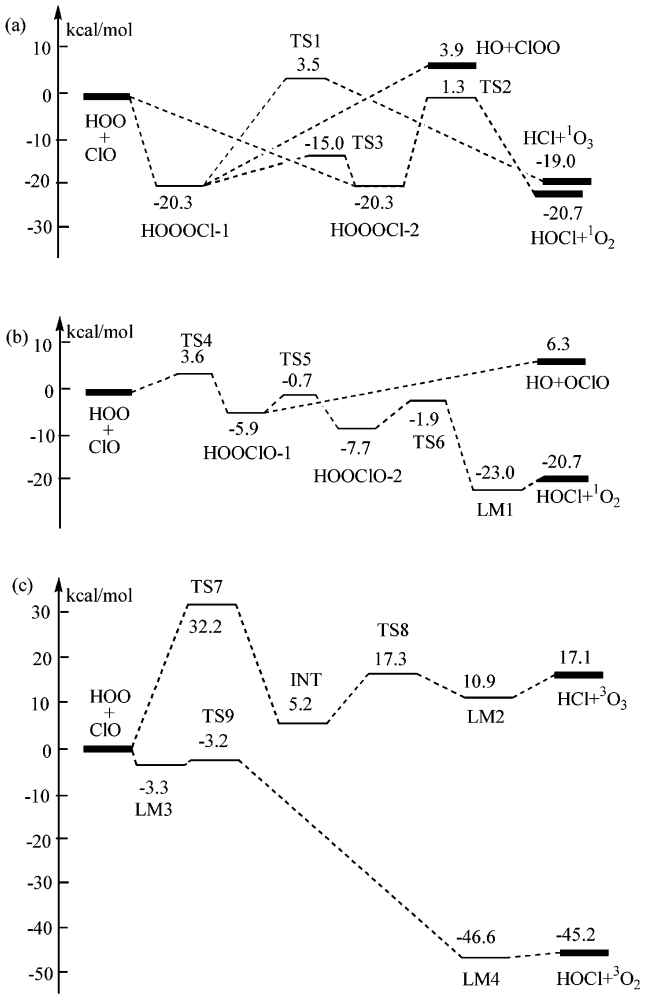

Figure 4. Schematic energy diagram of the HOO + ClO system at the G2M//B3LYP/6-311+G(3df, 2p) level, with the exception of the reaction channel of TS9 which was calculated at the G2M//BH&HLYP/6-311+G(3df, 2p) level. (a and b) singlet state PESs. (c) triplet state PES.

approaching each other, the reaction system goes over TS6 to the complex LM1. One can find that the distance of O(1)−H(5) shrinks rapidly to 1.363 Å at TS6 and that of Cl(2)−O(3) stretches by 0.473 Å from HOOClO-2 to TS6, and moreover, the dihedral angles ∠1234 and ∠2345 change from 79.2° and −91.9° in HOOClO-2 to 17.4° and −30.6° in TS6, respectively. Apparently TS6 is a twisted five-membered ring structure, whose geometry is similar to that optimized at the B3LYP/6-311++G(3df, 3pd) level by Nickolaisen et al.[10] LM1 is a typical hydrogen-bonding complex, whose H(3)−O(4) separation is 2.047 Å, and its geometric parameters are almost equal to those in the HOCl + $^1O_2$ products.

As shown in Figure 4b, TS4 is 3.6 kcal/mol over the reactants, and TS5 and TS6 are 0.7 kcal/mol and 1.9 kca.l/mol below the reactants, respectively. The relative energies of HOOClO-1 and HOOClO-2 are only −5.9 and −7.7 kcal/mol, respectively. The forward barriers of each step in the second channel are only 3.6, 5.2, and 5.8 kcal/mol corresponding to TS4, TS5, and TS6, respectively. So, the intermediates HOOClO-1 and HOOClO-2 are unstable in the HOO + ClO reaction system. The reaction is controlled by the first barrier, 3.6 kcal/mol, over which it should proceed favorably to the lower energy complex (LM1) lying 23.0 kcal/mol below the reactants.

(d) HO + OClO and HO + ClOO Formation. Besides the above stepwise channel, the excited HOOClO-1 can dissociate to form HO + OClO with 12.2 kcal/mol dissociation energy as shown in Figure 4b. Comparing the endothermicity of HO + OClO, 6.3 kcal/mol, with the energy of TS5, − 0.7 kcal/mol, one can expect that the formation of HO + OClO cannot compete with the formation of HOOClO-2, which produces HOCl + $^1O_2$ with facility. Similarly, the formation of HO + ClOO via the decomposition of the excited HOOOCl-1 also occurs with the endothermicity of 3.9 kcal/mol. This process is competitive with the formation of HOCl + $^1O_2$ and HCl + O_3.

2. Triplet Reaction Channels. (a) HCl + $^3O_3$ Formation. In principle, triplet O_3 can be formed by a two-step mechanism. In the first step, the reaction occurs via TS7 producing the intermediate INT, which is a five-member-ring triplet complex; its decomposition over TS8 leads to the hydrogen-bonding complex LM2. From Figures 1 and 2, one can see that the forming bond O(2)−O(3) is 1.587 Å in TS7 and 1.271 Å in INT, and the breaking bonds Cl(1)−O(2) are 1.889, 2.449, and 2.891 Å in TS7, INT, and TS8, respectively. The results show that the transfer of O atom from ClO to HOO mainly happens in the first step and the H migration from O(4) to Cl(1) occurs in the second step. In the order of INT, TS8, and LM2, the H(5)−O(4) distance changes from 0.991 to 2.192 Å to 2.332 Å and the H(5)−Cl(1) shortens from 2.114 to 1.287 Å to 1.284

TABLE 4: Heats of Formation of Five Species (in kcal/mol) at 0 K Predicted at the G2M Level

species	predicted values: this work[a]	predicted values: literature	expt.[30]
$^1O_3$	31.2 ± 0.9		34.1
HOCl ($^1A'$)	−17.0 ± 0.8	−16.0[16]	−17.1 ± 0.5
OClO($^2B_1$)	25.7 ± 0.8	25.3,[16] 24.7,[38] 28.2[39]	23.9 ± 1.9
ClOO	23.3 ± 0.8	23.5,[16] 23.1,[38] 30.2[39]	23.8 ± 0.7
HOOOCl	7.9 ± 0.8, 6.1 ± 1.9,[b] 8.4 ± 0.7[c]	9.1,[40] 12.5[10]	

[a] Evaluated on the basis of predicted heats of reaction and the heats of formation of ClO, HOO, OH, and HCl: 24.2 ± 0.02, 4.0 ± 0.8, 8.8 ± 0.007, and −22.0 ± 0.05 kcal/mol, respectively, taken from refs 30, 34, and 33. The errors in the predicted heats of formation only reflect those of experimental reference heats of formation. [b] Based on the enthalpy change for HOOOCl → HO + OClO using the experimental heats of formation of OH and OClO. [c] Based on the enthalpy change for HOOOCl → HO + ClOO using the experimental heats of formation of OH and ClOO.

TABLE 5: Energies of LMs, Transition States, and Products for HOO + ClO → HOCl + $^3O_2$ Relative to the Reactants with ZPE Corrections Based on the Geometries Optimized at the BH&HLYP, MP2, and QCISD Levels of Theory

calculation methods	relative energies (kcal/mol): LM3	TS9	LM4	HOCl + $^3O_2$
BH&HLY/6-311+G(3df,2p)	−3.0	−0.3	−42.6	−42.3
G2M//BH&HLY/6-311+G(3df,2p)	−3.3	−3.2	−46.6	−45.2
MP2/6-311+G(3df,2p)[a]	−4.0	−2.3	−63.3	−62.0
QCISD/6-311++G(d, p)[a]	−3.9	1.0	−48.2	−46.8

[a] Energies without ZPE correction.

Å. Apparently, LM2 is a hydrogen-bonding complex as mentioned above, and its geometric parameters are very close to those in the separate molecules of HCl and $^3O_3$. On account of the high barrier of 32.2 kcal/mol at the entrance step, the reaction is kinetically unimportant.

(b) HOCl + $^3O_2$ Formation. For this most exothermic product channel, we optimized the transition state (TS9) and two hydrogen-bonding complexes (LM3 and LM4) at the BH&HLYP level of theory with the 6-311+G(3df, 2p) basis set, because TS9 and LM3 could not be determined at the B3LYP level of theory as alluded to before. To confirm the existence of both TS9 and LM3 on the triplet potential energy surface, high-level electron correlation methods, MP2, QCISD, and CCD, with different basis sets were used to further optimize their structures. The optimized geometric parameters of LM3 and TS9 at different levels are displayed in Figure 3. Although the predicted structures are somewhat method-dependent, their existence has been confirmed, and the structures obtained at the BH&HLYP/6-311+G(3df,2p) level agree with those predicted by ab initio methods, such as the MP2/6-31G(d, p) method used by Toohey and Anderson[13] and by Buttar and Hirst[14] and the MP2/6-31G-(d) and CCSD(T)/6-31G(d) methods employed by Nickolaisen et al.[10] At the BH&HLYP/6-311+G(3df,2p) level, the forming bond O(2)−H(3) is 1.956 Å at LM3 and 1.415 Å at TS9, whereas the breaking bond H(3)−O(4) is 0.965 Å at LM3 and 1.040 Å at TS9, as shown in Figure 3. Thus, TS9 is a more reactant-like transition state. For LM4, the forming bond O(2)−H(3) and the breaking bond H(3)−O(4) are 0.955 and 2.271 Å at the BH&HLYP/6-311+G(3df, 2p) level, respectively (see Figure 1). Apparently, LM4 is a typical hydrogen-bonding complex composed of HOCl and $^3O_2$ molecules.

The relative energies obtained by various methods for all of the stationary points of this reaction channel are listed in Table 5. At the QCISD/6-311++G(d, p) level, the energy of TS9 is 1.0 kcal/mol higher than that of the reactants, whereas at the BH&HLYP/6-311+G(3df,2p), MP2/6-311+G(3df,2p), and G2M//BH&HLYP/6-311+ G(3df,2p) levels, their energies lie below the reactants by 0.3, 2.3, and 3.2 kcal/mol, respectively. The hydrogen abstraction barrier from LM3 to LM4 is only 0.1 kcal/mol at the G2M//BH&HLYP/6-311+G(3df,2p) level, compared with 2.7 kcal/mol before the G2M correction. LM4 and HOCl + $^3O_2$ have the relative energies of − 46.6 and − 45.2 kcal/mol, respectively, at the G2M//BH&HLYP/6-311+G(3df,2p) level. The latter is in good agreement with the experimental heat of reaction, − 45.3 kcal/mol.[30,34] These results basically agree those calculated by Nickolaisen et al.,[10] who reported the relative energies of LM3, TS9, and the products to be −2.8, −2.4, and −47.1 kcal/mol, respectively, at the CCSD(T)/6-311++G(2df,2p) level. Because of the small dissociation barrier and the large exothermicity for this channel, the high probability for the production of HOCl + $^3O_2$ can be expected. The structural parameters and energies obtained at the BH&HLYP/6-311+G(3df,2p) and G2M//BH&dHLYP/6-311+G(3df,2p) levels, respectively, will be used in the rate constant calculation for this channel. It should be mentioned that the trans counterpart of TS9, which was reported to be about 3 kcal/mol above the cis structure (TS9),[10] could not be found in our search, both at the UMP2 level with 6-31G(d) and 6-311G(d, p) basis sets and at the BH&HLYP/6-311+G(3df, 2p) level of theory.

To assess the reliability of our calculation, the predicted heats of formation of major species including HOOOCl are compared with experimental and other predicted values in Table 4. The predicted values, except $^1O_3$, agree reasonably with experimental and other predicted data; the differences between the available experimental and calculated values are less than 1.8 kcal/mol at the G2M level, which is within the combined experimental and predictive errors, estimated to be about ±2 kcal/mol for the present system.

B. Rate Constant Calculations. The rate constants for these reaction channels were calculated by using variational TST and RRKM rate theory using the energetics given in Figure 4 and the vibrational frequencies and moments of inertia given in Tables 2 and 3. The Lennard-Jones parameters required for the collisional stabilization of HOOOCl isomers are taken to be $\epsilon/k = 230$ K and $\sigma = 4.3$ Å from our previous paper[17] and the Lennard-Jones parameters for He and N_2 were taken from the literature.[41]

1. Abstraction Reaction. The rate constant for the production of HOCl + $^3O_2$ by abstraction was calculated in the temperature range from 150 to 2000 K with the VARIFLEX code.[24] As the reaction occurs barrierlessly via LM3, the $O_2H\cdots OCl$ complex, the potential energies along the MEP to the complex summarized in Table 6 were fitted to the Morse function with $D_e = 4.5$ kcal/mol and $\beta = 1.71$ Å^{-1}. As shown in Figure 5, the fitting is quite good and the error introduced by the use of the fitted function in our rate constant in this case is less than 1%. The rate constants calculated with and without including multiple reflections above the well of the complex were essentially the

TABLE 6: Energy Changes Relative to the Dissociating Intermediates along MEPs at Different O−O Separations for Four Reactions[a,b]

HOOOCl → HOO + ClO		HOOOCl → HO + ClOO		LM3 → HOO + ClO		HOOCl O-1 → HO + OClO	
R_{O-O} (Å)	ΔE (kcal/mol)	R_{O-O} (Å)	ΔE (kcal/mol)	R_{H-O} (Å)	ΔE (kcal/mol)	R_{O-O} (Å)	ΔE (kcal/mol)
1.4	0.62	1.5	0.93	2.1	0.10	1.4	0.04
1.5	3.90	1.6	5.57	2.2	0.34	1.5	2.10
1.6	8.51	1.7	12.14	2.3	0.66	1.6	5.96
1.7	13.60	1.8	19.65	2.4	1.02	1.7	10.20
1.8	18.95	1.9	21.21	2.5	1.37	1.8	14.06
1.9	20.79	2.0	21.51	2.6	1.70	1.9	14.40
2.0	21.56	2.1	21.75	2.7	2.00	2.0	14.59
2.1	21.79	2.2	21.56	2.8	2.27	2.1	14.64
2.2	21.79	2.3	21.56	2.9	2.53	2.3	14.50
2.3	21.94	2.4	21.69	3.0	2.75	2.4	14.55
2.4	22.04	2.5	21.91	3.2	3.12	2.6	14.75
2.6	22.28	2.6	21.97	3.4	3.40	2.7	14.86
2.9	22.67	2.7	22.39	3.6	3.56	2.8	14.97
		2.8	22.59	3.8	3.72	3.0	15.16
		2.9	22.77	4.0	3.83		
		3.0	22.95	4.3	3.96		
				4.5	4.03		

[a] The energies given above have been scaled to the dissociation energies of the intermediates computed at the G2M level (see footnote b to this table). All except the dissociation of LM3 were optimized at B3LYP/6-311G(d, p). The dissociation of LM3 was optimized at the BH&HLYP/6-311+G(3df, 2p) level as described in the text. [b] The errors incurred by the scaling, substituting the less reliable D_e values predicted by DFT calculations with the more reliable G2M energies in the two most important association reactions, $HO_2 + ClO \rightarrow$ LM1/LM2 and LM3, because of the difference between the DFT and G2M energies (see Table 5), were calculated to be less than 5% and 1%, respectively, because of the small energy differences near the dissociation limits which control the association processes. For the formation of LM3, the difference between the two energies is 0.3 kcal/mol as shown in Figure 5 and Table 5.

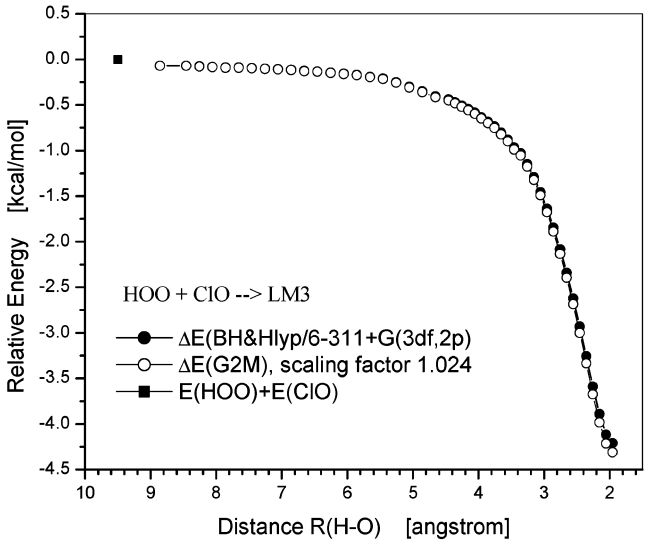

Figure 5. Comparison of the fitted Morse curve and the predicted $V(r)$ as a function of the OOH−OCl separation during the formation of LM3 with and without scaling of the predicted dissociation energies.

same and could be reasonably represented by the expression

$$k(\mathrm{HOCl}+{}^3\mathrm{O}_2) = 1.64 \times 10^{-10}\, T^{-0.64} \times \exp(107/T)\ \mathrm{cm}^3\,\mathrm{molecule}^{-1}\,\mathrm{s}^{-1}$$

for the temperature range 150−1000 K. The result corresponds to the measured $HO_2 + ClO$ rate constant at low pressures under which the formation of HOOOCl by stabilization is insignificant.

It is worth noting that the "direct" abstraction rate constant exhibits noticeable negative temperature dependence, attributable to the presence of TS9 which effectively reduces the incoming flux as the temperature of the system increases. If the PES evaluated by B3LYP, which failed to predict the presence of LM3 and TS9, was employed in our rate constant calculation, the absolute value of $k(HOCl + O_2)$ was found to be larger by a factor of 10 with negligible temperature dependence, contrary to experimental findings.

SCHEME 1

$$\mathrm{HOO + ClO} \leftrightarrow \mathrm{HOOOCl\text{-}1^*} \rightarrow \mathrm{HOOOCl\text{-}1\ (+M)}$$
$$\rightarrow \mathrm{HO + ClOO}$$
$$\rightarrow \mathrm{HCl + {}^1O_3}$$
$$\leftrightarrow \mathrm{HOOOCl\text{-}2^*} \rightarrow \mathrm{HOOOCl\text{-}2\ (+M)}$$
$$\rightarrow \mathrm{HOCl + {}^1O_2}$$
$$\rightarrow \mathrm{HOO + ClO}$$

SCHEME 2

$$\mathrm{HOO + ClO} \leftrightarrow \mathrm{HOOOCl\text{-}2^*} \rightarrow \mathrm{HOOOCl\text{-}2\ (+M)}$$
$$\rightarrow \mathrm{HOCl + {}^1O_2}$$
$$\leftrightarrow \mathrm{HOOOCl\text{-}1^*} \rightarrow \mathrm{HOOOCl\text{-}1\ (+M)}$$
$$\rightarrow \mathrm{HCl + {}^1O_3}$$
$$\rightarrow \mathrm{HOO + ClO}$$

SCHEME 3

$$\mathrm{HOO + ClO} \leftrightarrow \mathrm{HOOClO\text{-}1^*} \rightarrow \mathrm{HOOClO\text{-}1\ (+M)}$$
$$\rightarrow \mathrm{HO + OClO}$$
$$\leftrightarrow \mathrm{HOOClO\text{-}2^*} \rightarrow \mathrm{HOOClO\text{-}2\ (+M)}$$
$$\rightarrow \mathrm{HOCl + {}^1O_2}$$

2. Association/Decomposition Reactions. The rate constants for the product channels taking place via the HOOOCl-1 and HOOOCl-2 were computed with the ChemRate code[26] coupling all intermediates involved in the forward and reverse reactions as shown below.

(a) HOOOCl Formation and Decomposition. Because of the stability of HOOOCl-1 and HOOOCl-2 as aforementioned, it

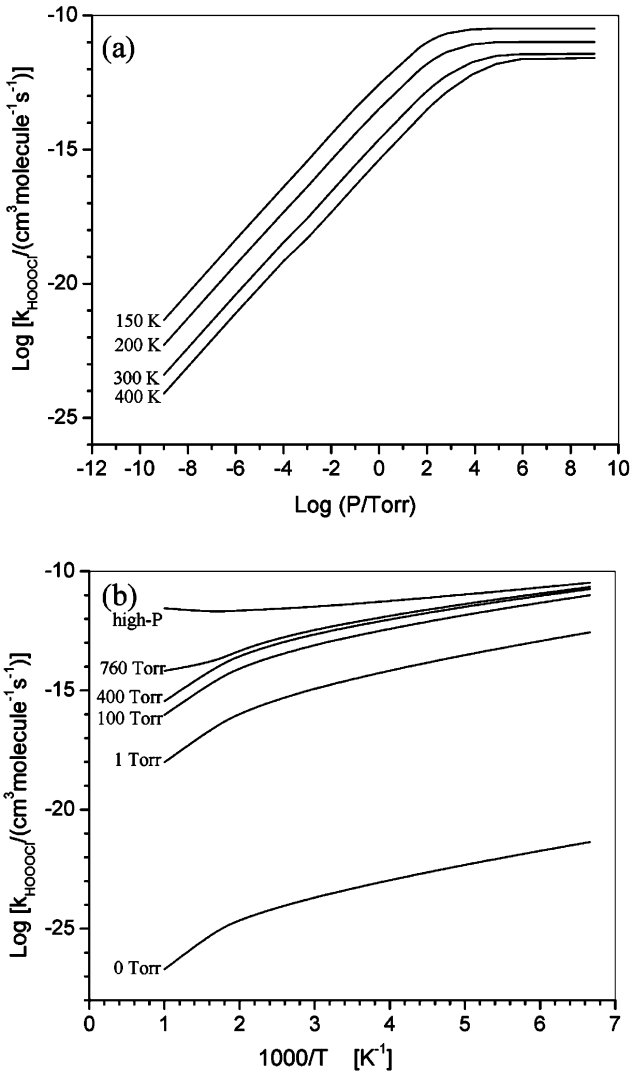

Figure 6. Plots of rate constants for the HOOOCl product channel with respect to temperature and pressure.

is necessary to calculate the rate constants for their stabilization. For the barrierless association processes leading to their formation, the energies at different O(2)−O(3) separations along the MEP paths were calculated by full optimization at the B3LYP/6-311G(d, p) level, and the transition state at each temperature was determined canonically based on the maximum Gibbs free energy criterion[42−44] for RRKM calculations using the ChemRate program. The predicted potential energies at different O(2)−O(3) separations are listed in Table 6 for both association channels producing HOOOCl-1 and HOOOCl-2. For the present system, the critical O(2)−O(3) separations in both association reactions were found to be somewhat insensitive to temperature, 1.95 Å below 1000 K and 1.90 Å above 1000 K. Because of the rapid isomerization reaction between both excited isomers formed by the association processes, the two isomers were treated as a single HOOOCl intermediate in our canonical variational RRKM calculations according to Schemes 1 and 2. The energy increment was fixed at 10 cm^{-1} in all sum-of-state and density-of-state calculations, and the energy grain size of either 50 or 100 cm^{-1} (with essentially the same result) was used in the master equation computation with the ChemRate program. Figure 6a shows the plots for the sum of association rate constants predicted by the two schemes at several temperatures for the pressure range 1×10^{-9}−1×10^{9} Torr. Fitting these $k-P$ curves using the following empirical equations[45,46]

$$k_a = a[b/(1+b)]F$$

$$\log F = \log F_c/[1+(\log b)^2]$$

with the predicted high- and low-pressure limits for N_2 as the third body gave rise to the broadening parameters $F_c = 0.55$, 0.52, 0.42, and 0.34 at 150, 200, 300, and 400 K, respectively. In the above fitting, $a = k_a^{\infty} = 9.04 \times 10^{-17}\ T^{1.22} \exp(897/T)$ cm^3 $molecule^{-1}$ s^{-1} and $b = k_a^0$ [M]/k^{∞} with $k_a^0 = 9.33 \times 10^{-24}\ T^{-3.45} \exp(472/T)$ cm^6 $molecule^{-2}$ s^{-1}. The predicted total rate constants for HOOOCl formation as functions of temperature at different pressures are presented in Figure 6b. The small increase in the association rate above 500 K at $P \geq 760$ Torr results essentially from the fast increase in the partition functions of the flexible transition state with temperature. The contribution of HOOOCl formation to the observed total rate constants is significant as will be discussed below.

Rate constants for the decomposition of HOOOCl under similar conditions as given above for the association process, producing predominantly $HO_2 + ClO$, can be represented by

$$k_d^0 = 2.69 \times 10^4\ T^{-3.51} \exp(-9770/T)\ cm^3\ molecule^{-1}\ s^{-1}$$

$$k_d^{\infty} = 5.68 \times 10^{12}\ T^{0.62} \exp(-9440/T)\ s^{-1}$$

The low-pressure data predict that, at 50 Torr N_2 pressure, the lifetime of HOOOCl at 200 K is about 270 days, whereas at 250 K, it reduces to about 1 h. Accordingly, the photochemistry of HOOOCl in the lower stratosphere may be relevant to the O_3-removal process.

(b) Formation of HCl + O_3, HOCl + $^1O_2$ and HO + ClOO via HOOOCl. At temperatures above 500 K, the three product channels with higher energy barriers involved in Schemes 1 and 2 become nonnegligible, although they are not significantly competitive with the abstraction channel until $T > 1000$ K. For the production of HO + ClOO occurring without a well-defined barrier (see Table 6), canonical variational transition states are located at the O(3)−O(4) separation of 2.1−2.0 Å at 200−800 K and slowly reduced to 1.8 Å above 1200 K. In Figure 7a, the rate constants for the formation of these product pairs, including HCl + O_3 (which have been reported experimentally) are compared with those for HOCl + $^3O_2$ and HOOOCl formation at 1 and 400 Torr. Apparently, below room temperature, formation of HOOOCl at 1 Torr pressure is more important than those minor product channels giving O_3, $^1O_2$, and ClOO, whose rate constants are pressure-independent. At 400 Torr, the average pressure employed by Nickolaisen et al.,[10] HOOOCl formation amounts to about 17% of the abstraction product yield at 200 K and about 1% at 400 K.

(c) Formation of HO + OClO and HOCl + $^1O_2$ via HOOClO. Once they are formed, both HOOClO-1 and HOOClO-2 intermediates fragment readily to these two product pairs. Their rate-limiting step lies in the relatively high barrier for their formation at TS4 (3.6 kcal/mol). Because of this barrier, formation of these products cannot compete with the HOCl + $^3O_2$ and HOOOCl product channels occurring without barriers. The decomposition of HOOClO-1 to HO + OClO also occurs without a distinct barrier (see Table 6), and its transition states are canonically located at the O(3)−O(4) distance of 1.9 Å below 1500 K and at 1.8 Å above that temperature. The result of ChemRate calculations based on Scheme 3, shown in Figure 7a, indicates that both product channels are comparatively insignificant to the observed $HO_2 + ClO$ rate constant as more

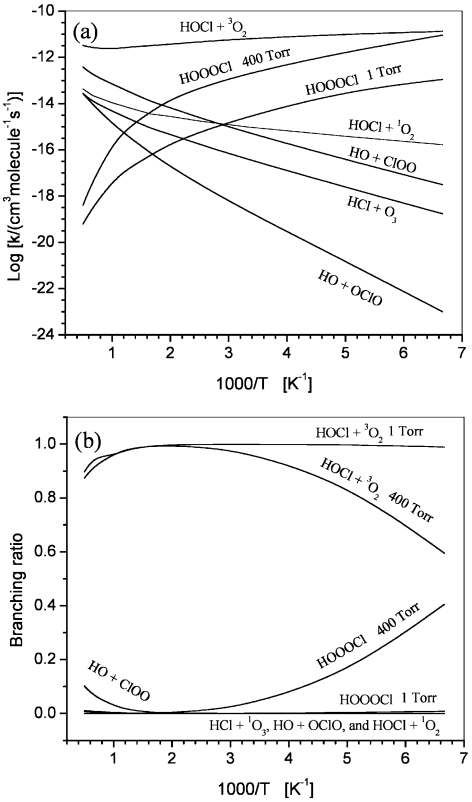

Figure 7. Plots of predicted rate constants for the HOO + ClO reaction as a function of temperature reciprocal. (a) Rate constants for individual product channels. (b) Branching ratios of individual product channels.

clearly illustrated by the product branching ratio plots presented below. For practical combustion applications, the rate constants for these bimolecular product channels have been evaluated in units of cm^3 molecule^{-1} s^{-1} for the 500−2500 K temperature range:

$$k(\mathrm{HOCl} + {}^3\mathrm{O}_2) = 1.30 \times 10^{-20}\, T^{2.37} \exp(-2572/T)$$

$$k(\mathrm{HOCl} + {}^1\mathrm{O}_2) = 1.39 \times 10^{-21}\, T^{2.26} \exp(226/T)$$

$$k(\mathrm{HO} + \mathrm{ClOO}) = 7.61 \times 10^{-19}\, T^{1.80} \exp(-1065/T)$$

$$k(\mathrm{HO} + \mathrm{OClO}) = 2.22 \times 10^{-21}\, T^{2.32} \exp(-2566/T)$$

$$k(\mathrm{HCl} + {}^1\mathrm{O}_3) = 7.60 \times 10^{-21}\, T^{2.05} \exp(-855/T)$$

(d) Product Branching Ratios. The branching ratios for all product channels are shown in Figure 7b as functions of temperature for 1 and 400 Torr N_2 pressure. At 1 Torr pressure, the HO_2 + ClO reaction occurs exclusively by abstraction producing HOCl + $^3O_2$. This conclusion supports the most recent result of Knight et al.,[11] who reported that HOCl was the only product of the reaction and no evidence for HCl + O_3 formation was observed in their experiment under 1.1−1.7 Torr pressure conditions. At 400 Torr pressure, the stabilization of HOOOCl becomes significant and competitive with the abstraction channel, amounting to about 15% of the total rate at 200 K and rapidly decreases to less than 4% at room temperature because of the fast increasing back reaction. The potential contribution of HOOOCl formation was first pointed out by Nickolaisen et al.[10] as mentioned before.

Our results are not consistent with the prediction of Tooley and Anderson[13] and the measurement of Finkbeiner et al.[9] The former suggested that the direct hydrogen abstraction channel should dominate at high temperatures, whereas the indirect elimination from the cyclic HOOClO intermediate would dominate at lower temperatures. The latter reported a branching ratio for the HCl + O_3 product channel up to as high as 5% at low temperatures according to their experimental measurement, inconsistent with our prediction and the observation of Knight et al.[11] as alluded to above.

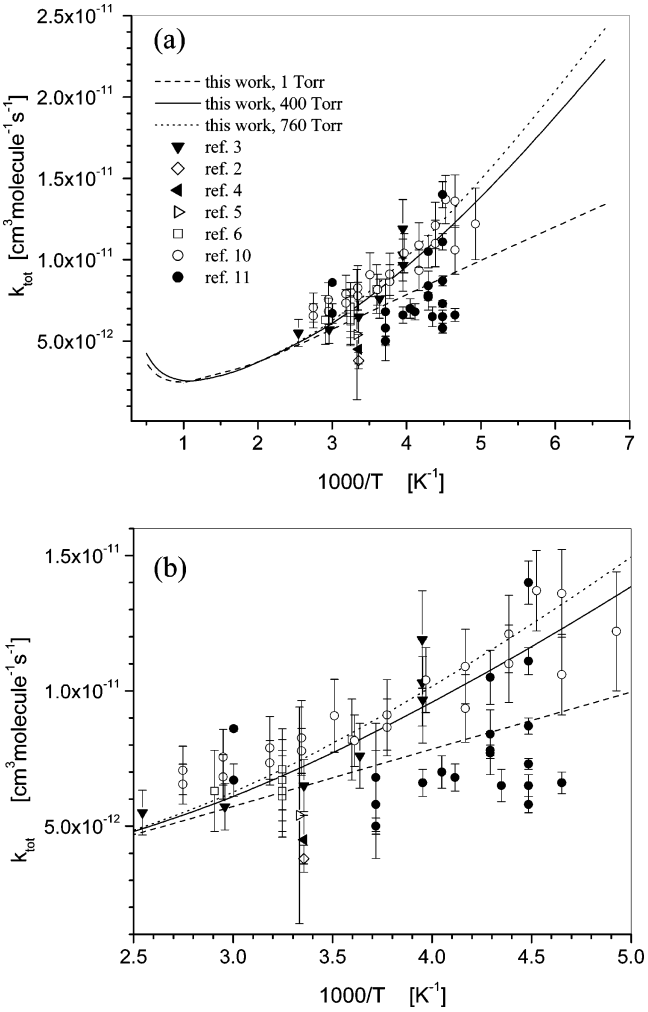

Figure 8. Comparison of the predicted total rate constants with the experimental data. (a) Rate constants in the temperature range from 150 to 2000 K; (b) The close-up of rate constants in the temperature range from 200 to 400 K.

(e) Total Rate Constant. The Arrhenius plots of predicted total rate constants at 1, 400, and 760 Torr pressures for HO_2 + ClO are compared with all existing experimental data in Figure 8. The predicted values lie within the scatter of experimental data with correct temperature dependence. Below room temperature, the total rate constant increases with pressure, attributable to the *P*-dependent contribution from HOOOCl formation. At 1 Torr pressure, the abstraction process accounts for nearly 100% of the observed rate as concluded above. The predicted value agrees closer with the results reported by Knight et al.[11] obtained at 1.1−1.7 Torr pressure with He as a carrier gas, $k(T) = (7.1 \pm 0.4) \times 10^{-12} \exp[(-16 \pm 17)/T]$ cm^3 molecule^{-1} s^{-1}. At 400 Torr N_2 pressure, the predicted total rate constant agrees closely with those of Nicklaisen et al.,[10] $k(T) = 2.84 \times 10^{-12} \exp[(312 \pm 60)/T]$ cm^3 molecule^{-1} s^{-1}. Our results also agree well with the data of Stimple et al.[3] and Cattell and Cox.[6] The values obtained by Reimann and

Kaufman,[2] Leck et al.,[4] and Burrows and Cox[5] are, however, somewhat lower than the predicted value.

The predicted total rate constants can be expressed in units of cm^3 $molecule^{-1}$ s^{-1} by the following equations for the temperature range 150−1000 K:

$$k(\mathrm{T}) = 1.97 \times 10^{-10}\, T^{-0.66} \exp(100/T) \text{ at 1 Torr}$$

$$k(\mathrm{T}) = 3.66 \times 10^{-11}\, T^{-0.45} \exp(270/T) \text{ at 400 Torr}$$

$$k(\mathrm{T}) = 3.52 \times 10^{-11}\, T^{-0.45} \exp(288/T) \text{ at 760 Torr.}$$

IV. Conclusions

The kinetics and mechanism for the HO_2 + ClO reaction system have been investigated at the G2M level of theory in conjunction with VTST and RRKM rate constant calculations. On the singlet PES, the reaction takes place via two isomers of HOOOCl which lie 20.3 kcal/mol below the reactants. At temperatures below 500 K, the collisional stabilization of HOOOCl accounts significantly for the observed rate constant and the formation of higher-barrier products such as HCl + O_3, HOCl + $^1O_2$, and HO + ClOO/OClO cannot compete with HOOOCl formation at $P > 1$ Torr. On the triplet PES, the direct abstraction reaction producing HOCl + $^3O_2$ is the overall most favorable channel; this highly exothermic ($\Delta H = -45.2$ kcal/mol) process occurs via a $O_2H\cdots OCl$ complex, with a 3.3 kcal/mol binding energy and a 0.1 kcal/mol decomposition barrier leading to product formation. The theoretically predicted total rate constants at 200 K < T < 400 K and 1−760 Torr pressure agrees satisfactorily with existing experimental data, exhibiting a strong negative temperature dependence below 1000 K.

On account of the reasonable stability of the HOOOCl intermediate at low temperatures (T < 250 K), its photochemistry in the lower stratosphere might affect the O_3-destruction process to some extent.

Acknowledgment. This work is sponsored by the Office of Naval Research under Contract No. N00014-02-1-0133, Dr. J. Goldwasser program manager.

References and Notes

(1) Wayne, R. P. *Chemistry of Atmospheres*, 2nd ed.; Clarendon Press: Oxford, U.K., 1991.
(2) Reimann, B.; Kaufman, F. *J. Chem. Phys*. **1978**, *69*, 2925.
(3) Stimpfle, R. M.; Perry, R. A.; Howard, C. J. *J. Chem. Phys*. **1979**, *71*, 5183.
(4) Leck, T. J.; Cook, J.-E. L.; Birks, J. W. *J. Chem. Phys*. **1980**, *72*, 2364.
(5) Burrows, J.; Cox, R. A. *J. Chem. Soc., Faraday Trans. 1* **1981**, *77*, 2465.
(6) Cattell, F. C.; Cox, R. A. *J. Chem. Soc., Faraday Trans. 2*. **1986**, *82*, 1413.
(7) Leu, M.-T. *Geophys. Res. Lett.* **1980**, *7*, 173.
(8) Kou, Y.-P.; Ju, S.-S.; Lee, Y.-P. *J. Chin. Chem. Soc*. **1987**, *34*, 161.
(9) Finkbeiner, M.; Crowley, J. N.; Horie, O.; Mueller, R.; Moortgat, G. K.; Crutzen, P. J. *J. Phys. Chem.* **1995**, *99*, 16264.
(10) Nickolaisen, S. L.; Roehl, C. M.; Blakeley, L. K.; Friedl, R. R.; Francisco, J. S.; Liu, R.; Sander, S. P. *J. Phys. Chem. A* **2000**, *104*, 308.
(11) Knight, G. P.; Beiderhase, T.; Helleis, F.; Moortgat, G. K.; Crowley, J. N. *J. Phys. Chem. A* **2000**, *104*, 1674.
(12) Mozurkewich, M. *J. Phys. Chem.* **1986**, *90*, 2216.
(13) Toohey, D. W.; Anderson, J. G. *J. Phys. Chem.* **1989**, *93*, 1049.
(14) Buttar, D.; Hirst, D. M. *J. Chem. Soc., Faraday Trans*. **1994**, *90*, 1811.
(15) Zhu, R. S.; Lin, M. C. *PhysChemComm* **2001**, *25*, 1.
(16) Zhu, R. S.; Xu, Z. F.; Lin, M. C. *J. Chem. Phys.* **2002**, *116*, 7452.
(17) Xu, Z. F.; Zhu, R. S.; Lin, M. C. *J. Phys. Chem. A* **2003**, *107*, 1040.
(18) Poulet, G.; Zagogianni, H.; Le Bras, G. *Int. J. Chem. Kinet*. **1986**, *18*, 847.
(19) Mebel, A. M.; Morokuma, K.; Lin, M. C. *J. Chem. Phys*. **1995**, *103*, 7414.
(20) (a) Becke, A. D.; *J. Chem. Phys*. **1993**, *98*, 5648. (b) Becke, A. D. *J. Chem. Phys.* **1992**, *96*, 2155. (c) Becke, A. D. *J. Chem. Phys.* **1992**, *97*, 9173.
(21) Lee, C.; Yang, W.; Parr, R. G. *Phys. Rev.* **1988**, *37B*, 785.
(22) (a) Gonzalez, C.; Schlegel, H. B. *J. Chem. Phys.* **1989**, *90*, 2154. (b) Gonzalez, C.; Schlegel, H. B. *J. Phys. Chem.* **1990**, *94*, 5523.
(23) Frisch, M. J.; Trucks, G. W.; Schlegel, H. B.; Scuseria, G. E.; Robb, M. A.; Cheeseman, J. R.; Zakrzewski, V. G.; Montgomery, J. A., Jr.; Stratmann, R. E.; Burant, J. C.; Dapprich, S.; Millam, J. M.; Daniels, A. D.; Kudin, K. N.; Strain, M. C.; Farkas, O.; Tomasi, J.; Barone, V.; Cossi, M.; Cammi, R.; Mennucci, B.; Pomelli, C.; Adamo, C.; Clifford, S.; Ochterski, J.; Petersson, G. A.; Ayala, P. Y.; Cui, Q.; Morokuma, K.; Malick, D. K.; Rabuck, A. D.; Raghavachari, K.; Foresman, J. B.; Cioslowski, J.; Ortiz, J. V.; Stefanov, B. B.; Liu, G.; Liashenko, A.; Piskorz, P.; Komaromi, I.; Gomperts, R.; Martin, R. L.; Fox, D. J.; Keith, T.; Al-Laham, M. A.; Peng, C. Y.; Nanayakkara, A.; Gonzalez, C.; Challacombe, M.; Gill, P. M. W.; Johnson, B. G.; Chen, W.; Wong, M. W.; Andres, J. L.; Head-Gordon, M.; Replogle, E. S.; Pople, J. A. *Gaussian 98*; Gaussian, Inc.: Pittsburgh, PA, 1998.
(24) Klippenstein, S. J.; Wagner, A. F.; Dunbar, R. C.; Wardlaw, D. M.; Robertson, S. H. *VARIFLEX*, version 1.00; 1999.
(25) Wardlaw, D. M.; Marcus, R. A. *Chem. Phys. Lett*. **1984**, *110*, 230; *J. Chem. Phys*. **1985**, *83*, 3462. Klippenstein, S. J. *J. Chem. Phys*. **1992**, *96*, 367. Klippenstein, S. J.; Marcus, R. A. *J. Chem. Phys.* **1987**, *87*, 3410.
(26) Mokrushin, V.; Bedanov, V.; Tsang, W.; Zachariah, M. R.; Knyazev, V. D. *ChemRate*, version 1.19; National Institute of Standards and Technology: Gaithersburg, MD, 2002.
(27) Uehara, H.; Kawaguchi, K.; Hirota, E. *J. Chem. Phys*. **1985**, *83*, 5479.
(28) Chase, M. W., Jr. NIST-JANAF Thermochemical Tables, 4th ed. *J. Phys. Chem. Ref. Data* **1998**, Monograph No. 9.
(29) Escribano, R. M.; Lonnardo, G. D.; Fusina, L. *Chem. Phys. Lett*. **1996**, *259*, 614.
(30) Huber, K. P.; Herzberg, G. *Molecular Spectra and Molecular Structure. IV. Constants of Diatomic Molecules*; Van Nostrand Reinhold Company: New York, 1979; p 716.
(31) Azzolini, C.; Cavazza, F.; Crovetti, G.; Dilonardo, G.; Frulla, R.; Escribano, R.; Fusina, L. *J. Mol. Spectroscopy* **1994**, *168*, 494.
(32) (a) Yamada, C.; Endo, Y.; Hirota, E. *J. Chem. Phys*. **1983**, *78*, 4379. (b) Burkholder, J. B.; Hammer, P. D.; Howard, C. J.; Towle, J. P.; Brown, J. M. *J. Mol. Spectrosc.* **1992**, *151*, 493.
(33) Ruscic, B.; Feller, D.; Dixon, D. A.; Peterson, K. A.; Harding, L. B.; Asher, R. L.; Wagner, A. F. *J. Phys. Chem. A* **2001**, *105*, 1.
(34) Litorja, M.; Ruscic, B. *J. Electron Spectrosc. Relat. Phenom*. **1998**, *97*, 131.
(35) Peterson, K. A.; Francisco, J. S. *J. Chem. Phys*. **2000**, *112*, 8483.
(36) Phillips, D. H.; Quelch, G. E. *J. Phys. Chem.* **1996**, *100*, 11270.
(37) Rohlfing, C. *Chem. Phys. Lett*. **1995**, *245*, 665.
(38) Zhu, R. S.; Lin, M. C. *J. Phys. Chem. A* **2002**, *106*, 8386.
(39) Li, W. K.; Ng, C. Y. *J. Phys. Chem*. A **1997**, *101*, 113.
(40) Francisco, J. S.; Sander, S. P. *J. Phys. Chem.* **1996**, *100*, 573.
(41) Hippler, H.; Troe, J.; Wendelken, H. J. *J. Chem. Phys.* **1983**, *78*, 6709.
(42) Isaacson, A. D.; Truhlar, D. C. *J. Chem. Phys*. **1982**, *76*, 1380.
(43) Hsu, C.-C.; Mebel, A. M.; Lin, M. C. *J. Chem. Phys*. **1996**, *105*, 2346.
(44) Chakraborty, D.; Hsu, C.-C.; Lin, M. C. *J. Chem. Phys*. **1998**, *109*, 8889.
(45) Troe, J. *J. Phys. Chem*. **1979**, *83*, 114.
(46) Troe, J. *Ber. Bunsen-Ges. Phys. Chem*. **1983**, *87*, 161. Gilbert, R. G.; Luther, K.; Troe, J. *Ber. Bunsen-Ges. Phys. Chem*. **1983**, *87*, 169.